Journal of Materials Chemistry C

PAPER

View Article Online
View Journal | View Issue

Cite this: J. Mater. Chem. C, 2016, 4, 2235

Insight into the effect of functional groups on visible-fluorescence emissions of graphene quantum dots†

Jianglin Du,[a] Haiyu Wang,*[a] Lei Wang,[a] Shoujun Zhu,[b] Yubin Song,[b] Bai Yang[b] and Hongbo Sun[a]

Received 5th February 2016,
Accepted 15th February 2016

DOI: 10.1039/c6tc00548a

www.rsc.org/MaterialsC

Graphene quantum dots (GQDs) with a variety of functional groups are studied by adjusting the pH of the solvents and through reduction using chemical methods. Our study suggests that the –CO–OH and $-CO-N(CH_3)_2$ groups could contribute to the green fluorescence emission (peak at 500–520 nm), and the $-CO-N(CH_3)_2$ group could form the green fluorescence emission state more effectively. Additionally, –OH groups and free zigzag sites may contribute to the blue fluorescence emission (peak at around 420 nm). The edge states and functional groups commonly constitute fluorescence emission centers. Additionally, both blue and green fluorescence emission centers corresponding to the molecule-like states could be quenched using the electron acceptor methyl viologen, which barely affects the intrinsic state of the carbon honeycomb flat structure.

1. Introduction

Graphene-based materials have drawn tremendous attention in recent years due to their superior electronic, thermal, and mechanical properties.[1–3] While graphene, graphene oxide (GO), and graphene oxide nanocolloid-sheets have become popular in physical and chemical domains, graphene quantum dots (GQDs) have been recently focused on due to their unique properties of low-toxicity, high-biocompatibility, and bright fluorescence emission.[4–7] GQDs, as a kind of graphene-based material, inherit some excellent physical attributes of graphene with the special structure of a single atomic layer of nano-sized graphite, such as high surface area, large diameter and better surface grafting using π–π bonding. Beyond that, various functional groups decorated on the surface cause GQDs to exhibit excellent solubility and availability for subsequent functionalization with other species. Nevertheless, in contrast to graphene, GQDs possess fascinating photoluminescence (PL) properties, for instance, high quantum yield, excitation wavelength-dependent emission, pH-sensitive luminescence intensity, and up-conversion PL.[4,8] These unique characteristics make GQDs perfect candidates for numerous exciting applications, *i.e.*, bioimaging, medical diagnosis, catalysis and photovoltaic devices.[9–13]

Recently, the concept of carbon light-emitting diodes (CLEDs) has gradually emerged. CLEDs may demonstrate much higher carrier transport mobility, longer life-times and better robustness compared with the currently available organic light-emitting diodes (OLEDs).[14,15] However, quantum yield improvement and the emitting wavelength design in fluorescent carbon nanomaterials still require the solution of a lot of fundamental problems. This limits the progress of CLED fabrication techniques. Hence, insight into the mechanism of the fascinating photoluminescence emission behaviors of fluorescent carbon nanomaterials could be the main key to achieve the goal of CLEDs with better optical characteristics in the future.

According to previous reports on PL behavior, reasonable mechanisms could refer to the intrinsic graphene core state and edge state.[15–19] For the GQDs with few surface chemical groups, theoretical calculations suggested that the perfect carbon-honeycomb flat structure produced the bandgap of π-domains which contributes to the PL emission.[20] That means the fluorescent emission wavelength is size-dependent. But some experimental results hardly supported this point of view, because both size-dependent and size-independent GQDs have been reported.[21,22] On the other hand, for GQDs with abundant functional groups, steady-state studies show that the PL centers may be located at edge site states and defect states including the hybrid structures formed by oxygen-containing functional groups at the edges or on the flats.[23,24] It is reported that $-NH_2$ groups can increase the quantum yield of GQDs,[25,26] and relevant theoretical calculations

[a] State Key Laboratory on Integrated Optoelectronics, College of Electronic Science and Engineering, Jilin University, Changchun, 130012, People's Republic of China. E-mail: haiyu_wang@jlu.edu.cn
[b] State Key Laboratory of Supramolecular Structure and Materials, Jilin University, Changchun, 130033, People's Republic of China

† Electronic supplementary information (ESI) available: Fig. S1–S5. See DOI: 10.1039/c6tc00548a

suggest that the bandgap of the GQDs decreases as $-NH_2$ groups are added.[27]

As femtosecond time-resolved methods have emerged to be powerful tools to research the PL mechanism of many new graphene materials,[28–33] recently, Wang *et al.* has proposed a PL scheme in green-fluorescence GQDs based on several time-resolved spectroscopies.[14] They have reported that green-fluorescence GQDs possess two kinds of bright molecule-like states, corresponding to green and blue fluorescence. Moreover, some other research has reported blue emission is from the electron transition of sp^2 domains.[34] Because these reports about the mechanism of fluorescence emissions in GQDs lead to different results, further detailed research should be carried out to help understand the origin of GQDs.

In this paper, we illustrate the effect of some functional groups on visible-fluorescence emissions of GQDs with high photo-luminescence quantum yields and abundant functional groups. By changing the pH of the GQD solutions and by reduction treatment using $NaBH_4$, specific functional-group-dependent fluorescence has been observed. For green fluorescence emission, the –CO–OH and $-CO-N(CH_3)_2$ groups could exert important actions, and N-containing functional groups, especially the $-CO-N(CH_3)_2$ group, could form green fluorescence emission states more effectively. As for blue fluorescence emission, the –OH and free zigzag sites states may form the main contribution. It is found that the deprotonation effect and various functional groups could influence the lifetime of the excited states corresponding to the fluorescence emissions using femtosecond transient absorption experiments. Additionally, we use the PL quenching method to investigate the related fluorescence states and the charge transfer processes in GQDs, which has been adopted to explore the electronic states in carbon dots (CDs).[35–37] With the electron-acceptor methyl viologen (MV^{2+}) as the quencher,[38,39] it is found that the fluorescence emissions of GQDs can be effectively quenched by MV^{2+}, whose reduction potential level is between molecule-like states and the intrinsic state.

2. Experimental

2.1 Sample synthesis

Green fluorescence GQDs were provided by Professor Yang's group, which were synthesized using a reported method.[7,8,34] The freeze-dried GO was dispersed in DMF with a concentration of 50 mg/10 mL. The GO/DMF solutions were ultra-sonicated for 30 minutes, and then transferred to a poly(Teflon)-lined autoclave and heated at 200 °C for 8 h. After filtering, the brown liquid containing GQDs can be obtained. The GQDs were purified using column chromatography on silica utilizing gradient elution (methylene chloride–MeOH (1 : 1, v/v)). Then we obtained relatively pure GQDs with the size of several nanometers. To change the pH of the GQDs, HCl and NaOH were added to the water solutions of the GQDs to adjust the pH to 0 and 14, respectively. We choose DMF, THF, methanol, and water to compare the solvent effects. Reduced GQDs were prepared by adding 50 mg of $NaBH_4$ to aqueous GQDs (0.1–1 mg mL^{-1}), and stirring at room temperature for 4 hours.[34]

Graphene oxide nano-ribbons (GORs) with an abundance of –CO–OH groups were synthesized by unzipping Single Walled Carbon Nanotubes (SWCNTs).[40] A mixture of SWCNTs (50 mg) and 98% H_2SO_4 (75 mL) was ultra-sonicated for 20 minutes and stirred overnight. $KMnO_4$ (250 mg) was then added in several portions with stirring for 2 hours. After that, the mixture was stirred at 70 °C for 2 more hours, and in the meantime, extra $KMnO_4$ (100 mg) was added slowly causing the color to change from dark to violet-red. After cooling down, 250 mL of water and 5 mL of H_2O_2 were added to the mixture in an ice-bath to dilute the H_2SO_4 and stop the reaction. Finally, the dispersion was centrifuged (6000 rpm, 20 min) to discard unreacted SWCNTs. Because the solvent was acid, the GOR dispersion was dialyzed for one week to neutralize the solvent. M-GORs were prepared by adding NH_4OH (20 mL) to the GOR dispersion (40 mL), and the mixture was stirred at 75 °C for 2 hours. GOR-QDs were synthesized like GQDs. GOR dispersions (200 mL) were evaporated to get solid GORs. And solid GORs were dispersed in 50 mL of DMF using ultra-sonication for 30 minutes. Then, the mixture was transferred to a poly(Teflon)-lined autoclave and heated at 200 °C for 8 h. After filtering, the brown liquid containing GOR-QDs could be obtained.

2.2 Femtosecond transient absorption setup

The TA setup consisted of 400 nm pump pulses doubled from 800 nm laser pulses ($\sim$100 fs duration, 250 Hz repetition rate) generated from a mode-locked Ti:sapphire laser/amplifier system (Solstice, Spectra-Physics) and broadband white-light probe pulses generated from 2 mm-thick deuterated water. The relative polarization of the pump and the probe beams was set to the magic angle. The TA data were collected by a fiber-coupled spectrometer connected to a computer. The group velocity dispersion of the transient spectra was compensated for using a chirp program. All the measurements were performed at room temperature. Pump-power dependent measurements were carried out. In the acceptable range, no pump intensity dependent dynamics were observed.

3. Results and discussion

Fig. 1a shows the schematic of the green-fluorescence GQD groups which were prepared through a top-bottom method (quantum yield is 11.4%).[7] The carbon plate with defects acts as a core of the GQD, and various functional groups are linked onto it. The –OH, =O and –CO–OH groups originate from the graphene oxide synthesized by the modified Hummers method, and the $-CO-N(CH_3)_2$ groups are given by the dimethyl formamide (DMF) in the hydrothermal process. Fig. S1 (ESI†) shows the transmission electron microscope (TEM) image of the GQDs, and it indicates that the size of the GQDs was about several nanometers in diameter. Fig. 1b shows the absorption spectrum of the GQDs dissolved in water (named original GQDs). There is an obvious band in the absorption spectrum, which is located at around 400 nm with a long tail. This corresponds to the previous report in which it is explained that the absorption

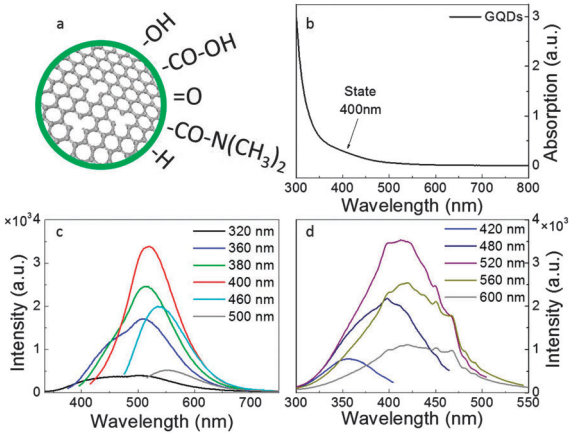

Fig. 1 (a) Schematic illustration of the functional groups in the GQDs. (b) Steady-state absorption of the GQDs. (c) PL spectra of the GQDs excited at 320–520 nm. (d) PL excitation spectra of the GQDs.

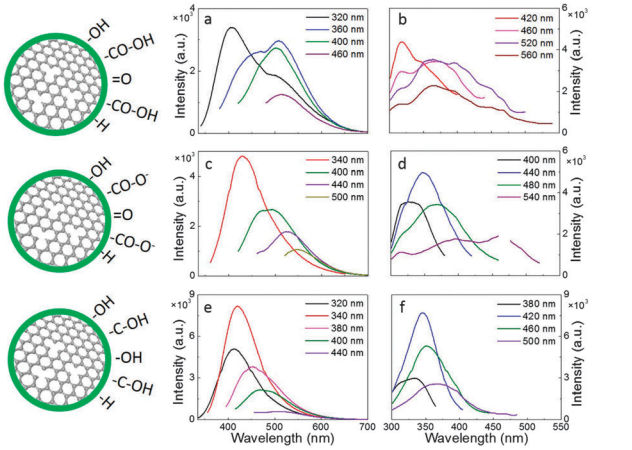

Fig. 2 Steady-state experiments on GQDs with different modifications. (a and b) PL spectra and PL excitation spectra of GQDs in pH = 0 solvents, (c and d) GQDs in pH = 14 solvents, and (e and f) r-GQDs.

band is due to the overlapping of carbon backbones and oxidation functional groups.[14] From the PL spectra and the PL excitation spectra in Fig. 1c and d, it can be seen that GQDs exhibit excitation-dependent PL behaviors. There is a weak peak at around 430 nm with a shoulder peak at 520 nm when excited at 320 nm. However, with the redshift of the excitation wavelength, a strong peak at 520 nm dominated and the 430 nm peak disappeared. From the PL excitation spectra, the main peak probed at 520 nm corresponds to the excitation wavelength at 400 nm which has also been shown in the absorption spectra. In the shorter excitation wavelength area, we can also find a state at around 360 nm contributing to the 430 nm fluorescence emission. Previous time resolved spectroscopy experimental results indicate that these two states are due to two kinds of molecule like states.[14] For the green fluorescence state there are special edge states consisting of several carbon atoms on the edge of the carbon backbone and functional groups containing C=O.[14]

Functional groups such as –OH, –CO–OH, and –CO–N$(CH_3)_2$ originate from the synthesis process.[14,34] In order to explore the effects of these different kinds of functional groups on the fluorescence emission, the pH value of the GQD solvent was changed from 7 to 0 and 14. The fluorescence spectra changed differently as Fig. 2 shows. When the solvent pH value was adjusted from 7 to 0 by adding HCl, the intensity of the fluorescence of the GQDs decreased in the 480–550 nm range. However, the 400 nm peak (excited at 320 nm) became comparable with the 520 nm peak (excited at 400 nm). As shown in the PL excitation spectra (Fig. 2b), the intensity of the original 400 nm excitation state decreased to lower than that of the 320 nm state which corresponds to the 400 nm emission in Fig. 2a. A detailed comparison with the 520 nm peak in the previous PL spectra of the original GQDs implies that the green emission peak moves little as the excitation wavelength increases when the GQDs are in a solution with pH = 0 (360 nm to 460 nm). Next, when the pH value of the solvent was changed from 7 to 14 by adding NaOH, the intensity of the green-fluorescence decreased more, and the 430 nm peak became dominating while the 520 nm peak almost vanished. The dominance of the state at 360 nm is also be evident from the PL excitation spectra in Fig. 2d. Additionally, an obvious peak at 540 nm (excited at 460 nm) at pH = 14 appeared which seems different from the previous 520 nm peak of the original GQDs. Furthermore, NaBH can reduce the carbonyl group and transform it to –OH accompanied by decreased surface defects. In the NaBH reduced GQD (r-GQD) PL spectra (Fig. 2e), blue emission (430 nm) increased remarkably and became the major peak, while the longer wavelength emission portion disappeared. And the PL excitation spectra (Fig. 2f) also shows that the dominant 340 nm state corresponding to the 420 nm emission in Fig. 2e became much higher, while there was no obvious peaks in the long wavelength range.

The –OH groups are relatively more difficult to ionize than the –CO–OH and –CO–N$(CH_3)_2$ groups, so they are more stable in the chemical modifications. As seen in Fig. S2 (ESI†), in the Fourier Transform Infrared (FTIR) spectra, the –OH feature peak at 3200–3600 nm is almost unchanged between the pH = 7, pH = 0 and pH = 14 solvents. But the other functional groups below 1700 nm are more active. In the pH = 0 solvent, part of the –CO–N$(CH_3)_2$ group could be hydrolyzed by an H^+ ion and changed to –COOH while the –OH and –CO–OH groups suffered little effect. We could assume that the –CO–N$(CH_3)_2$ group makes a partial contribution to the 520 nm emission. By carefully observing the PL spectra, the green fluorescent peak of pH = 0 sample was narrower and located at 505 nm. That means that the –CO–N$(CH_3)_2$ group could bring a broad fluorescence emission at around 500–540 nm. In another situation, the –CO–OH group could be deprotonated to –CO–O^- in pH 14 solvent and additionally, part of the –CO–N$(CH_3)_2$ group could also be hydrolyzed to –CO–O^-. Since the intensity of the green fluorescence peak (520 nm) was further decreased in pH = 14 compared to the partial decrease in pH = 0, we can infer that the –CO–OH group also plays a conclusive role in the 520 nm emission. Thus, combining the fixed 505 nm emission originating from the –CO–OH group and the broad range (500–540 nm) emission from the –CO–N$(CH_3)_2$ group, the derivation of the green-fluorescence

emission in GQDs could be deduced. On the other hand, the –OH group which was almost unchanged in the pH = 0 and pH = 14 solvents may contribute to the blue fluorescence emission at 430 nm, which agrees with the previous report that –OH contributes to the blue emission in carbon nanomaterials.[41] $NaBH_4$ could reduce the carbon–oxygen double bond to a carbon–oxygen single bond,[34] so part of the =O, –CO–OH and –CO–$N(CH_3)_2$ groups could be reduced to –OH and –CH_2–OH groups. From the PL spectra, excitation-dependent PL behavior of the reduced GQDs (r-GQDs) is similar to that of the GQDs in the pH = 14 solvent. The PL peak at 520 nm almost disappeared alongside the remarkable increase of the 430 nm peak due to the increase of the number of –OH groups (corresponding to the increase of the peak at 3200–3600 nm in the FTIR spectra as Fig. S1, ESI† showed), which also supports the concept that the –OH groups contribute to blue-fluorescence emission. However, one different phenomenon is that the 540 nm fluorescence peak emerging in the pH = 14 solvent cannot be observed in r-GQDs either from the PL spectra or the excitation spectra.

By comparing the steady-state behavior of the r-GQDs with that of the GQDs at pH = 14, we can infer that the –OH group in both of the samples may contribute to the 430 nm fluorescence emission, but the effects of the transformed functional groups from the –CO–OH group, –CH_2–OH in the r-GQDs and –CO–O^- in pH = 14 solvents, could be different. According to the PL emission spectra excited at the 460 nm state and the excitation spectra probed at 540 nm (Fig. 2c and d), we can suggest that the new fluorescence peak emerging at 540 nm at pH = 14 could be due to the –CO–O^- group. Because the 540 nm fluorescence peak is much weaker than the original 520 nm fluorescence peak, the –CO–O^- group state may possess a lower fluorescence quantum yield. And another interesting feature in the pH = 14 solvent is that the amount of –OH groups didn't increase but the blue emission at 430 nm was a little enhanced. In consideration of the deprotonation effect in the pH = 14 solvent, the amount of free zigzag sites could be increased, which were reported as blue-fluorescence emission centers in GQDs.[29] So the blue-fluorescence emission could also be contributed by the edge states. Combining the above results, the preliminary conclusion is that different surface groups lead to different fluorescence emission from 430 nm to 540 nm: both –OH groups and free zigzag site states contribute to blue fluorescence emission (430 nm), –CO–OH and –CO–$N(CH_3)_2$ groups together contribute to green fluorescence emission (520 nm) with a high quantum yield, and deprotonated –CO–O^- groups contribute to green fluorescence emission (540 nm) with a low quantum yield.

To further confirm the key roles of the –CO–OH and –CO–$N(CH_3)_2$ groups, we did another experiment, which focused on graphene nanoribbon.[42,43] In some recent research, it has been proposed that the fluorescence properties of carbon-nanomaterials (like CDs and GQDs) mainly depend on functional groups instead of particle size like traditional semiconductor quantum dots.[15,32,44] That means the fluorescence emission state in carbon-nanomaterials may have a common origin. So, in order to investigate the fluorescence properties of GQDs, we could investigate a kind of GOR with abundant –CO–OH groups at the edge to help us understand the distinction between the –CO–OH and –CO–$N(CH_3)_2$ groups.[40] Fig. S3a (ESI†) shows a TEM image of GORs, and they twisted into a cluster after being unzipped from the nanotubes. As seen in the X-ray photoelectron spectroscopy (XPS) in Fig. 3a, there were three main peaks corresponding to the C–C, C–O, and –CO–OH moieties. The more obvious peak at 283 eV for the GORs compared to that of the reported GO confirmed that there were many more –CO–OH groups.[45] Fig. 3b shows the PL spectra of the GORs: the main fluorescence emission peak was at 400 nm (under 300 nm excitation), and the emission intensity at 500 nm was so weak that we almost could not identify it. Then, we modified GORs (M-GORs) with –NH_2 groups by adding NH_4OH at 75 °C for two hours. XPS in Fig. 3c shows that the N1s peak (red sign) of the M-GORs at 400 eV was higher than that of the GORs, which corresponded to a higher N content (12.18%) in the M-GORs than in the GORs (3.39%). That means the element N had been successfully linked with the GORs. Interestingly, after the –NH_2 group was involved, the PL spectra (Fig. 3d) of the M-GORs produced a weak but distinct emission peak at 500 nm under about 400 nm excitation. Next, in order to investigate the effect of the –$N(CH_3)_2$ group, we further modified GORs with DMF. Under high temperature (200 °C), DMF would decompose to form a –$N(CH_3)_2$ group. Meanwhile, GORs could be linked with it and were separated into nanometer debris to form GOR quantum dots (GOR-QDs). Fig. S3b (ESI†) shows that the size of the GOR-QDs was similar to that of previous GQDs, which was about several nanometers. After these treatments, the green fluorescence emission at 520 nm is much stronger than for the M-GORs (as shown in Fig. 3e, the quantum yield is about 11%). Also the excitation-dependent fluorescence properties of the

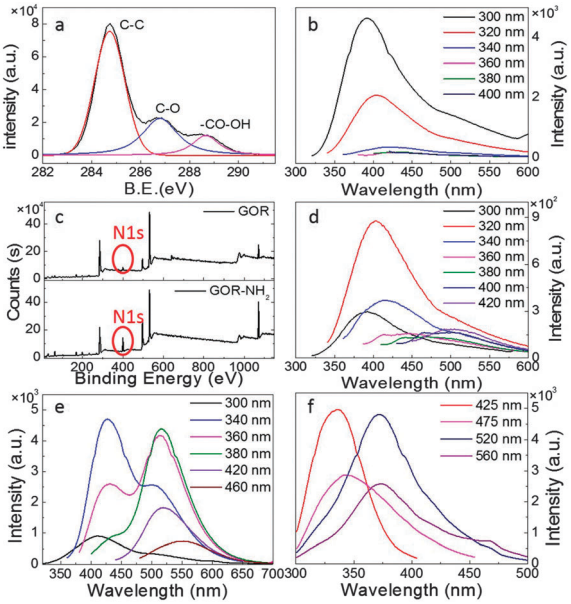

Fig. 3 Steady-state experiments on the GORs, M-GORs and GOR-QDs. (a) XPS (C1s) of the GORs. (b) PL spectra of the GORs. (c) XPS of the GORs and M-GORs. (d) PL spectra of the M-GORs. (e and f) PL spectra and PL excitation spectra of the GOR-QDs.

GOR-QDs are similar to those of the GQDs. Two main distinct emission states at 425 nm and 520 nm could also be identified in the excitation spectra (Fig. 3f) corresponding to the 325 nm and 375 nm excitation.

The above experiment showed that the GORs with abundant –CO–OH groups could not emit green fluorescence effectively. But NH_4OH could change part of the –CO–OH groups into –CO–NH_2 groups at temperatures over 75 °C. With the appearance of the –CO–NH_2 group, M-GORs could emit green fluorescence slightly. That means that the –NH_2 group could contribute more to the green fluorescence emission (500 nm) than the –CO–OH group. Additionally, GOR-QDs with the –$N(CH_3)_2$ group showed a strong green fluorescence emission, whose fluorescence property was similar to that of the previous GQDs synthesized from graphene. From these GOR related experiments, we deduced that the element N could be the key point to form green fluorescence emission (520 nm) centers more effectively than the –CO–OH group in either GORs or GQDs. And in N containing functional groups, the –$N(CH_3)_2$ group could contribute more green fluorescence emission than the –NH_2 group. This conclusion is in agreement with a previous report, which proposed a synthesis of blue fluorescent GQDs by cage-opening C_{60}.[46] They chemically treated blue GQDs with hydrazine hydrate to form N-containing moieties. The hydrazine-reduced GQDs showed a red-shift emission maximum from 450 nm to 520 nm, which also indicated that the element N could contribute to green fluorescence emission. Thus, we could make a comprehensive understanding about various functional groups and the corresponding fluorescence emissions in GQDs.

Nevertheless, steady fluorescence spectra can only provide limited information about the fluorescence excited states of the GQDs, so additionally, we explored the ultrafast dynamics properties of the excited states using femtosecond broadband transient absorption (TA) spectroscopy. First, a different sample of GQDs was excited at 400 nm as Fig. 4 shows. The photo-excited electrons in the excited states could further absorb probe light to higher levels or return to the ground state by stimulated radiation due to the disturbance of the probe light, known as so-called excited-state absorption (ESA) and stimulated emission (SE). Fig. 4a shows the TA spectra of the GQDs, and we can observe a strong ESA at 475 nm and a SE at around 530 nm corresponding to the state of green fluorescence emission.[30] For GQDs in the pH = 14 and pH = 0 solvents and the r-GQDs, the TA spectra shows weaker SEs than for the original GQDs and similar ESAs with a little wavelength shift (Fig. 4b–d). That means that the change in functional groups could slightly affect the fluorescence states in the GQDs. However, by comparing the kinetics of the ESAs in different GQD samples, we could find that the decay rates of the ESAs in the GQDs varies with different functional group modifications during the first several picoseconds. By changing the pH of the solvents and through the reduction process, the partial radiative emission state in the GQDs (from the –CO–OH and –CO–$N(CH_3)_2$ groups) could be transformed to other states (from the –CO–O^- and –OH groups), which are non-radiative states and become electron trapping states. Thus, these radiative states and nonradiative states could form a competition

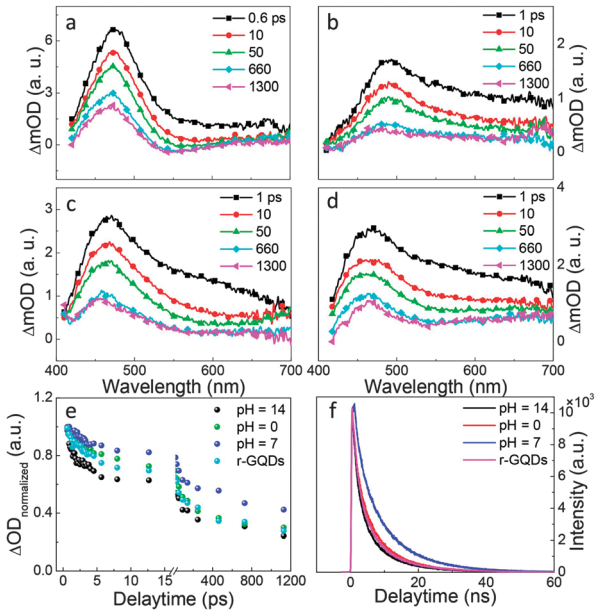

Fig. 4 Transient-state experiments on GQDs. TA spectra excited at 400 nm for (a) GQDs in water, (b) GQDs in pH = 14 solvents, (c) GQDs in pH = 0 solvents, and (d) r-GQDs. (e) Kinetics comparison of the ESAs of the GQDs in four conditions. (f) PL dynamics of the GQDs in four conditions using TCSPC experiments.

relation, and the trapping states could speed up the decay of the excited states. As the experimental results showed, the lifetime of the ESAs in the modified GQDs were shorter than original GQDs in the picosecond range. On the other hand, over the long-time range (nanosecond), the excited states obviously decay faster after the functional groups have been changed, while there are little variations between modified samples. The lifetime of the fluorescence of the GQDs has been measured by time-correlated single-photon counting (TCSPC) experiments. In Fig. 4f, the lifetimes of the fluorescence excited at 405 nm were obtained. The lifetime of the original GQDs was obviously longer than the others, and the other three modified GQDs possess similar fluorescence lifetimes, which corresponds to both the decrease in the fluorescence intensity excited at 400 nm in the steady-state PL experiments and the lifetime changes of the excited states in the TA experiments over the nanosecond range. Combining the above results and the previous reports, we infer that the functional groups linked at the edge of the carbon plates could form fluorescence emission states, whose energy levels depend on the kind of functional groups.

The above experiments mainly focused on the properties of the fluorescence emission states, which are relative energy levels in GQDs. Since GQDs have many applications in photovoltaic and photocatalytic fields,[47,48] it is important to know their absolute energy levels. In order to investigate the absolute energy levels and charge transfer processes, we further performed a PL quenching experiment on the GQDs. A MV^{2+} water solution (1 mol L^{-1}) was used to be the fluorescence quencher. As MV^{2+} was added into the GQD samples, the fluorescence intensity of the GQDs decreased (Fig. 5a). When the concentration of added

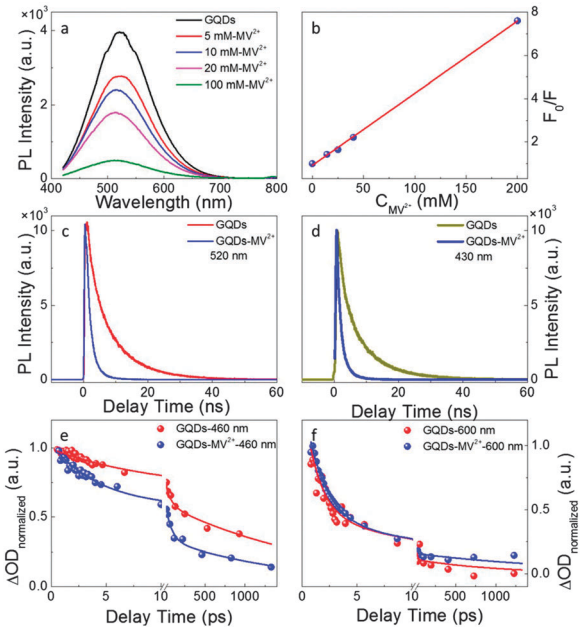

Fig. 5 (a) Steady-state PL spectra excited at 400 nm with MV^{2+} added of GQDs. (b) Stern–Volmer plots of GQDs. (c) PL dynamics of the GQDs at 520 nm and (d) 430 nm using TCSPC experiments. (e) Transient absorption dynamics of featured ESA signals in GQDs at 460 nm and (f) 600 nm. The dots are experimental results and the lines are fitting curves.

MV^{2+} reached 200 mM, the fluorescence of the GQDs was quenched in excess of 90%. Detailed calculations were needed to investigate this effect.

The fluorescence intensity quenching data is treated with the Stern–Volmer (SV) equation:[49,50]

$$\frac{F_0}{F} = 1 + K_{SV}[Q]$$

F and F_0 are the fluorescence intensities with and without quencher respectively, Q is the quencher, and K_{SV} is the SV quenching constant. When the dynamic quenching dominates the process, $K_{SV} = k_q\tau_{ave}$, where τ_{ave} is the average fluorescence lifetime of the excited-state fluorophore, and k_q is the bimolecular quenching rate constant. When the quenching is dominated by the static process, $K_{SV} = K_a$, where K_a is the association constant for the formation of the ground-state fluorophore–quencher complex.

In the SV plots, the fluorescence intensity was plotted *versus* the quencher concentration, as shown in Fig. 5b. A linear relationship for the fluorescence intensity *versus* the MV^{2+} concentration is obtained, which means the fluorescence quenching is dominated by a purely static or dynamic pathway. The experimental result for K_{SV} was 33 M^{-1}.

The fluorescence lifetimes are measured using the TCSPC system (Fig. 5c and d). Using two-exponential fitting, the satisfactory fitting lifetimes of the fluorescence state are shown in Table 1. The lifetime for the 430 nm fluorescence emission is 4.8 ns, and the lifetime for the 520 nm fluorescence is 6.1 ns. When 200 mM MV^{2+} was added, the green (520 nm) and blue (430 nm) fluorescence lifetimes were 4–5 times shorter than those without the addition of MV^{2+}. Hence, it is a dynamic quenching process in the GQDs mixed with a high concentration (200 mM) of MV^{2+}. On the other hand, the SV equation could also be used to distinguish the dynamic and static quenching processes. Since in principle k_q cannot exceed the diffusion rate constant $k_{diffusion}$ (*ca.* 8×10^9 M^{-1} s^{-1} for MV^{2+}) when quenching is fully dynamic,[37] based on the obtained τ_{ave} = 6.1 ns at 520 nm for the GQD–MV^{2+} hybrid, an upper limit of K_{SV} is $K_{SV\text{-}Maximum} = k_{diffusion}\tau_{ave} = 8 \times 10^9$ M^{-1} $s^{-1} \times 6.1$ ns = 48.8 M^{-1}. In the SV plots, the obtained K_{SV} was lower than $K_{SV\text{-}Maximum}$, so the quenching process in the GQD–MV^{2+} hybrid could also be confirmed to be dominated by the dynamic mechanism.

Table 1 Multi-exponential fitting of the TCSPC data for the GQDs before and after MV^{2+} was added

Exp.	τ_1/ns	τ_2/ns	τ_{ave}/ns
GQD			
430 nm	1.6(54%)	8.5(46%)	4.8
520 nm	2.2(51%)	10.2(49%)	6.1
GQD + MV^{2+}			
430 nm	0.4(56%)	2.2(44%)	1.2
520 nm	1.1(81%)	3.2(19%)	1.5

In order to investigate the excited-state variations of GQDs and GQD–MV^{2+} hybrid samples during the quenching process, femtosecond transient absorption was used to gain more information. Fig. S4 (ESI†) shows the transient absorption spectra of GQDs with added MV^{2+}. For pure GQD solutions (Fig. 4a), there are two featured excited state absorptions (ESAs) at 460 nm and 600 nm which have been discussed before,[14] but for the GQD–MV^{2+} hybrid solutions (Fig. S4, ESI†), there are larger ESA signals at 600 nm within the first several picoseconds than those in pure GQD solutions. Compared with the decay traces of GQDs at 460 nm, the molecule-like states decayed much faster after MV^{2+} was added (Fig. 5e). Whereas the decay traces of the intrinsic states at 600 nm are affected little by MV^{2+} in the first several picoseconds (Fig. 5f). Table 2 shows the satisfactory fitting lifetimes for Fig. 5e and f. For pure GQD solutions, the molecule-like state (460 nm) contains three lifetime compositions: τ_1 = 14 ps, τ_2 = 346 ps, and τ_3 = 6100 ps, where τ_3 is fixed to the average PL lifetime τ_{ave} for each component in Table 1. Thus, the average lifetime for the molecule-like states in pure GQDs is about 2720 ps. With MV^{2+} added, since all the lifetime components decrease remarkably, the average lifetime of the GQD–MV^{2+} hybrid becomes 566 ps, about 5 times shorter than that without the addition of MV^{2+}.

Table 2 Multi-exponential fitting of the featured ESA signals in GQDs before and after MV^{2+} is added

Exp.	τ_1/ps	τ_2/ps	τ_3/ps	τ_{ave}/ps
GQD				
460 nm	14(30%)	346(27%)	6100(43%)	2720
600 nm	2.3(99%)	135(1%)		2.4
GQD + MV^{2+}				
460 nm	4(40%)	75(27%)	1648(33%)	566
600 nm	2.8(99%)	2009(1%)		2.9

This is consistent with the green fluorescence lifetime change (520 nm), which further confirms that this molecule-like state (460 nm) is responsible for the green fluorescence of the GQDs. However, for the intrinsic states (600 nm), the average lifetimes are about 3 ps, remaining unchanged after MV^{2+} is added.

By analyzing the changes in the PL lifetimes and excited state lifetimes, we can obtain an integrated schematic illustration of the states in the hybrid GQD–MV^{2+} systems. At first, the reduction potential of MV^{2+} should be located below the excited-state energy level of the molecule-like state at 460 nm, so that the electrons in the high-energy excited states above the molecule-like state at 460 nm can be extracted by MV^{2+}. In the meantime, the reduction potential of MV^{2+} should be higher than the intrinsic states at 600 nm, since the excited electrons in the intrinsic states can decay to the ground state and barely feel the influence of MV^{2+}. The quenching experiments confirmed the assumption that the intrinsic state in the GQDs originated from the sp^2 (carbon-honeycomb flat) structure,[21] and the molecule-like states contained the functional groups located at the edge of the GQDs.[13]

4. Conclusions

We explore the visible-fluorescence behaviour of GQDs by adjusting their functional groups. The functional groups inherited from the graphene oxide are mainly –OH, –CO–OH, and –CO–$N(CH_3)_2$. With the change of pH value in the GQD solutions and the reduction treatment, the steady-state PL spectra varied clearly. Combined with the fluorescence properties of GORs, we deduce that the visible-fluorescence of GQDs originates from the functional groups which are linked up to the edge of the carbon-honeycomb flat structures. Functional groups and free zigzag site states may contribute to the blue-light emission, the –CO–$N(CH_3)_2$ groups may play the most important roles in green-light emission, and the –CO–O^- group may lead to a red-shift of the PL peak. Various functional groups directly constitute various fluorescence emission states, and nonradiative fluorescence states could form electron trapping states to compete with the radiative fluorescence emission states. By modulating the proper functional groups of GQDs, we could obtain various fluorescence properties of GQDs that contribute to achieving carbon-light-emitting devices. In the quenching experiment, MV^{2+} as an electron acceptor could effectively quench the fluorescence emission in GQDs. The steady-state and time-resolved PL studies demonstrated that it was dominated by a dynamic quenching process. Further femtosecond transient absorption experiments indicated the reduction potential of MV^{2+} was located between the excited-state energy levels of the molecule-like state at 460 nm and the intrinsic state at 600 nm. In addition, the charge transfer occurring from the GQDs to MV^{2+} could allow more applications in GQD-based photo-electron devices.

Acknowledgements

We would like to acknowledge the financial support from the 973 project (Grant #2014CB921302), Natural Science Foundation of China (NSFC Grant No. #21473077 and #21273096) and Doctoral Fund Ministry of Education of China (Grant #20130061110048).

References

1 A. K. Geim and K. S. Novoselov, *Nat. Mater.*, 2007, **6**, 183.
2 Y. L. Zhang, L. Guo, S. Wei, Y. Y. He, H. Xia, Q. D. Chen, H. B. Sun and F. S. Xiao, *Nano Today*, 2010, **5**, 15.
3 J. Y. Luo, L. J. Cote, V. C. Tung, A. T. L. Tan, P. E. Goins, J. S. Wu and J. X. Huang, *J. Am. Chem. Soc.*, 2011, **4**, 599.
4 J. H. Shen, Y. H. Zhu, X. L. Yang and C. Z. Li, *Chem. Commun.*, 2012, **48**, 3686.
5 D. Qu, M. Zheng, L. G. Zhang, H. F. Zhao, Z. G. Xie, X. B. Jing, R. E. Haddad, H. Y. Fan and Z. C. Sun, *Sci. Rep.*, 2015, **5**, 7998.
6 L. Wang, Y. L. Wang, T. Xu, H. B. Liao, C. J. Yao, Y. Liu, Z. Li, Z. W. Chen, D. Y. Pan, L. T. Sun and M. H. Wu, *Nat. Commun.*, 2014, **5**, 6357.
7 S. J. Zhu, J. H. Zhang, C. Y. Qiao, S. J. Tang, Y. F. Li, W. J. Yuan, B. Li, L. Tian, F. Liu and R. Hu, *Chem. Commun.*, 2011, **47**, 6858.
8 S. J. Zhu, S. J. Tang, J. H. Zhang and B. Yang, *Chem. Commun.*, 2012, **48**, 4527.
9 D. Y. Pan, J. C. Zhang, Z. Li, C. Wu, X. M. Yan and M. H. Wu, *Chem. Commun.*, 2010, **46**, 3681.
10 S. J. Zhuo, M. W. Shao and S. T. Lee, *ACS Nano*, 2012, **6**, 1059.
11 H. Shen, L. Zhang, M. Liu and Z. Zhang, *Theranostics*, 2012, **2**, e0013.
12 Y. Li, Y. Hu, Y. Zhao, G. Shi, L. Deng, Y. Hou and L. Qu, *Adv. Mater.*, 2011, **23**, 776.
13 X. Y. Zhang, Y. Zhang, Y. Wang, S. Kalytchuk, S. V. Kershaw, Y. H. Wang, P. Wang, T. Q. Zhang, Y. Zhao, H. Z. Zhang, T. Cui, Y. D. Wang, J. Zhao, W. W. Yu and A. L. Rogach, *ACS Nano*, 2013, **7**, 11234–11241.
14 L. Wang, S. J. Zhu, H. Y. Wang, Y. F. Wang, Y. W. Hao, J. H. Zhang, Q. D. Chen, Y. L. Zhang, W. Han, B. Yang and H. B. Sun, *Adv. Opt. Mater.*, 2013, **1**, 264.
15 S. J. Zhu, Y. B. Song, X. H. Zhao, J. R. Shao, J. H. Zhang and B. Yang, *Nano Res.*, 2015, **8**, 355–381.
16 K. P. Loh, Q. Bao, G. Eda and M. Chhowalla, *Nat. Chem.*, 2010, **2**, 1015.
17 M. L. Mueller, X. Yan, B. Dragnea and L. S. Li, *Nano Lett.*, 2011, **11**, 56.
18 M. L. Mueller, X. Yan, J. A. McGuire and L. S. Li, *Nano Lett.*, 2010, **10**, 2679.
19 P. Yang, L. G. Zhou, S. L. Zhang, N. Wan, W. Pan and W. Z. Shen, *J. Phys. Chem. C*, 2014, **116**, 244306.
20 G. Eda, Y. Y. Lin, C. Mattevi, H. Yamaguchi, H. A. Chen, I. S. Chen, C. W. Chen and M. Chhowalla, *Adv. Mater.*, 2010, **22**, 505–509.
21 J. Peng, W. Gao, B. K. Gupta, Z. Liu, R. Romero-Aburto, L. H. Ge, L. Song, L. B. Alemany, X. B. Zhan, G. H. Gao, S. A. Vithayathil, B. A. Kaipparettu, A. A. Marti, T. Hayashi, J. J. Zhu and P. M. Ajayan, *Nano Lett.*, 2012, **12**, 844.
22 L. B. Tang, R. B. Ji, X. K. Cao, J. X. Lin, H. X. Jiang, X. M. Li, K. S. Teng, C. M. Luk, S. J. Zeng, J. H. Hao and S. P. Lau, *ACS Nano*, 2012, **6**, 5102.

23 K. A. Ritter and J. W. Lyding, *Nat. Mater.*, 2009, **8**, 235–242.
24 Q. Xu, Q. Zhou, Z. Hua, Q. Xue, C. Zhang, X. Wang, D. Pan and M. Xiao, *ACS Nano*, 2013, **7**, 10654–10661.
25 H. Tetsuka, R. Asahi, A. Nagoya, K. Okamoto, I. Tajima, R. Ohta and A. Okamoto, *Adv. Mater.*, 2012, **24**, 5333–5338.
26 G. S. Kumar, R. Roy, D. Sen, U. K. Ghorai, R. Thapa, N. Mazumder, S. Saha and K. K. Chattopadhyay, *Nanoscale*, 2014, **6**, 3384–3391.
27 S. H. Jin, D. H. Kim, G. H. Jun, S. H. Hong and S. Jeon, *ACS Nano*, 2013, **7**, 1239–1245.
28 J. Y. Shi, C. Y. Chan and Y. T. Pang, *Biosens. Bioelectron.*, 2015, **67**, 595.
29 D. Y. Pan, J. C. Zhang, Z. Li and M. H. Wu, *Adv. Mater.*, 2010, **22**, 734.
30 X. Yan, X. Cui and L. S. Li, *J. Am. Chem. Soc.*, 2010, **132**, 5944.
31 L. Wang, H. Y. Wang, Y. Wang, S. J. Zhu, Y. L. Zhang, J. H. Zhang, Q. D. Chen, W. Han, H. L. Xu, B. Yang and H. B. Sun, *Adv. Mater.*, 2013, **25**, 6539–6545.
32 L. Wang, S. J. Zhu, H. Y. Wang, S. N. Qu, Y. L. Zhang, J. H. Zhang, Q. D. Chen, H. L. Xu, W. Han, B. Yang and H. B. Sun, *ACS Nano*, 2014, **8**, 2541.
33 L. Wang, Q. Li, H. Y. Wang, J. C. Huang, R. Zhang, Q. D. Chen, H. L. Xu, W. Han, Z. Z. Shao and H. B. Sun, *Light: Sci. Appl.*, 2015, **4**, e245.
34 S. J. Zhu, J. H. Zhang, S. J. Tang, C. Y. Qiao, L. Wang, H. Y. Wang, X. Liu, B. Li, Y. F. Li, W. L. Yu, X. F. Wang, H. C. Sun and B. Yang, *Adv. Funct. Mater.*, 2012, **22**, 4732.
35 Y. B. Song, S. J. Zhu, S. Y. Xiang, X. H. Zhao, J. H. Zhang, H. Zhang, Y. Fu and B. Yang, *Nanoscale*, 2014, **6**, 4676.
36 F. Lin, D. J. Pei, W. N. He, Z. X. Huang, Y. J. Huang and X. Q. Guo, *J. Mater. Chem.*, 2012, **22**, 11801.
37 V. Strauss, J. T. Margraf, C. Dolle, B. Butz, T. J. Nacken, J. Walter, W. Bauer, W. Peukert, E. Spiecker, T. Clark and D. M. Guldi, *J. Am. Chem. Soc.*, 2014, **136**, 17308.
38 Y. F. Wang, H. Y. Wang, Z. S. Li, J. Zhao, L. Wang, Q. D. Chen, W. Q. Wang and H. B. Sun, *J. Phys. Chem. C*, 2014, **118**, 17240.
39 F. E. Oddy, S. Brovelli, M. T. Stone, E. J. F. Klotz, F. Cacialli and H. L. Anderson, *J. Mater. Chem.*, 2009, **19**, 2846.
40 J. Liu, G. H. Kim, Y. H. Xue, J. Y. Kim, J. B. Baek, M. Durstock and L. Dai, *Adv. Mater.*, 2014, **26**, 786.
41 Q. S. Mei, K. Zhang, G. J. Guan, B. H. Liu, S. H. Wang and Z. P. Zhang, *Chem. Commun.*, 2010, **46**, 7319.
42 D. V. Kosynkin, A. L. Higginbotham, A. Sinitskii, J. R. Lomeda, A. Dimiev, B. K. Price and J. M. Tour, *Nature*, 2009, **458**, 872.
43 D. V. Kosynkin, W. Lu, A. Sinitskii, G. Pera, Z. Sun and J. M. Tour, *ACS Nano*, 2011, **5**, 968.
44 H. Ding, S. B. Yu, J. S. Wei and H. M. Xiong, *ACS Nano*, 2016, **10**, 484.
45 Y. H. Xue, H. Chen, D. S. Yu, S. Y. Wang, M. Yardeni, Q. B. Dai, M. M. Guo, Y. Liu, F. Lu, J. Qu and L. M. Dai, *Chem. Commun.*, 2011, **47**, 11689.
46 C. K. Chua, Z. Sofer, P. Simek, O. Jankovsky, K. Klimova, S. Bakardjieva, S. H. Kuckova and M. Pumera, *ACS Nano*, 2015, **9**, 2548.
47 V. Gupta, N. Chaudhary, R. Srivastava, G. D. Sharma, R. Bhardwaj and S. Chand, *J. Am. Chem. Soc.*, 2011, **133**, 9960.
48 R. F. Yeh, C. Y. Teng, S. J. Chen and H. S. Teng, *Adv. Mater.*, 2014, **26**, 3297.
49 C. Y. Tan, E. Alas, J. G. Muller, M. R. Pinto, V. D. Kleiman and K. S. Schanze, *J. Am. Chem. Soc.*, 2004, **126**, 13685.
50 K. Sun, H. B. Chen, L. Wang, S. Y. Yin, H. Y. Wang, G. X. Xu, D. N. Chen, X. J. Zhang, C. F. Wu and W. P. Qin, *ACS Appl. Mater. Interfaces*, 2014, **6**, 10802.

